Magnetic field structure and current formation during breakdown in TCV

Jonathan Rossel

February 2004

Assistant: Jean-Marc Moret
Sciences de base
CRPP, EPFL

Contents

1 Abstract

In the present report, we establish the foundations of a global process of data analysis, whose aim is to contribute to the understanding and enhancement of plasma breakdown in Tokamaks by the study of the magnetic field structure during this particular phase. We present how the application of a finely tuned linear regression can produce very robust results for the reconstruction of magnetic field maps, even with an initially low accuracy on the measurements. We also give a modelisation of the trajectory of the center of gravity of the plasma current, and we finally introduce the basis that will be used for a statistical treatment of the correlations between the minima of the magnetic field, the breakdown failure or achievement, and the initial position of the plasma.

2 Introduction

2.1 Basic phenomenology

The breakdown, in a plasma experiment, is the phase of plasma creation. This generally consists in setting an electric discharge in a gas by maintaining an electric tension on it. This tension will allow the propagation of the ionisation throughout the gas. In a Tokamak, like TCV (Tokamak à configuration variable), it is induced circularly by an ohmic transformer. A magnetic field is also set simultaneously to the breakdown in order to confine the plasma and to manipulate it. The stability of the magnetic confinement is difficult to control and rely on different passive devices and processes in addition to a closed-loop electronic control system. A crucial part of the equilibrium is assured by the magnetic field produced by the current circulating in the plasma itself. During the breakdown, this current does not exist, but there must already be a magnetic configuration as one cannot adjust the very moment of plasma creation and magnetic fields setting (which also takes time). Consequently, breakdown must occur in the presence of a magnetic field. However, if it were truly the case, plasma creation would be impossible because the proto-plasma (i.e. still not confined) would be rejected out of the high magnetic field regions. The trick is then to create zones of low intensity poloidal magnetic fields at the regions where we would like the plasma to appear, so that proto-plasma created anywhere else is lost by diffusion and only the part in the desired regions is allowed to propagate circularly.

2.2 Aims and objectives

The main aims of this project are to determine what are the magnetic features of the zones of plasma ignition, and what conditions must be fulfilled to obtain the desired breakdown with a good probability. To achieve these aims, we have first built a model giving the magnetic configuration and plasma current with their respective errors for any "shot" (complete experiment) in TCV, and implemented it in *Matlab*. This has allowed us to check the consistency of our model and will be used later on to complete the data basis of the shots with the generated results. In a second time, we have developed another program using the previous results to build a certain number of relevant parameters for each shot. These parameters are for example the minimum of the poloidal magnetic field (amplitude, position, area) at the breakdown time, or the trajectory of the plasma current center of gravity. They will be used later on as the basis of a statistical analysis, whose objectives are first to determine wether magnetic constraints are effectively relevant and decisive in breakdown achievement, secondly to determine their value and thirdly (eventually) to figure out what ensembles of parameters of TCV will fulfill these constraints.

2.3 Short description of TCV

To have a good understanding of the work exposed here, one has to have an idea of how TCV is built and how magnetic measurements are made. To have a more comprehensive presentation, see [1].

TCV is basically a stainless steel vacuum vessel with a set of coils and probes (see figure 1). The vessel has the shape of a torus and an almost rectangular section. There are three sets of coils. The first one forms the air core ohmic transformer (7 coils placed such that the produced magnetic field is nearly zero in the vessel). The second one consists in 2 stacks of 8 poloidal coils and allows the plasma shape control and the magnetic equilibrium. The 16 coils are independently power supplied. The last set is composed of 16 other coils producing a toroidal magnetic field. As far as probes are concerned, there are 4 cross-sections of the vessel (90° spaced) that are equipped with 38 magnetic probes measuring the component of the poloidal field tangential to the vacuum vessel. In the entirety of our treatment, cylindrical symmetry of the torus is assumed. In consequence, only one particular cross-section is studied and the values that are used are the averages of two of the four cross-sections (storing of the data from the four cross-sections has apparently been considered not to be useful). In addition to the magnetic probes, poloidal flux loops are wound on the outside of the

vacuum vessel. There is one loop per probe (for one section) and per shaping coil. The external transformer coils are also equipped with such coils. Nevertheless, in the present work, the loops corresponding to the coils have not been taken into account as the power supply system implies too much noise on them.

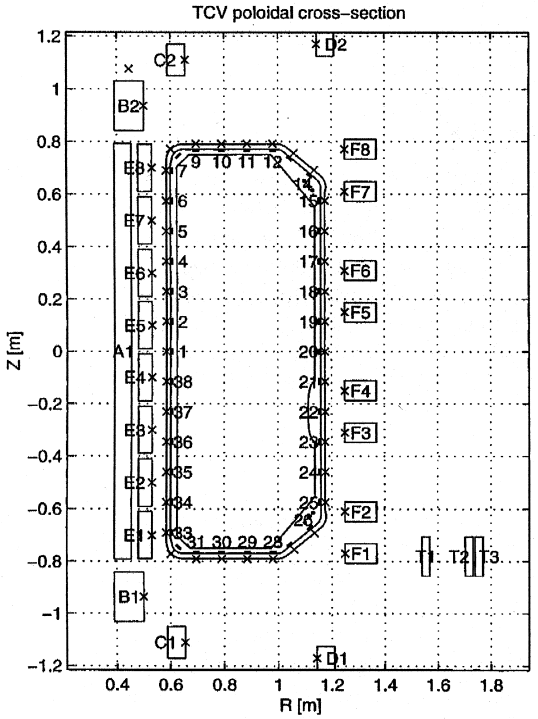

Figure 1: TCV poloidal cross section showing the ohmic transformer coil A, B, C, and D, the shaping coil E and F, the toroidal field coil connection T, the poloidal flux loops (×), and the magnetic field probes plotted as to scale rectangles in the vacuum vessel. Figure from J.-M. Moret *et al.* [1].

3 Modelisation for a generic case

3.1 Main principles

We expose here how the modelisation of the poloidal magnetic field and of the different currents is made. The approach used here rely extensively on the work done by [2]. The method consists in finding the currents and their derivatives in the poloidal coils (the three sets of coils), the vessel and the plasma by making a least square fitting of a combination of measurements and physical constraints. Currents and derivatives are treated as independent parameters at first (see section 3.2 for the complete treatment). The poloidal magnetic field is then found by a combination of the fitted currents and of geometrical parameters.

The formalism we adopt here is to group every measurement or unknown of the same kind in matrices, the rows of which are the different values in each group and the columns the different times of measurements. In the notations, repeated indices imply a diagonal matrix and indices inversion implies matrix inversion. Let us call the measured poloidal coils current I_a ($1 \leq a \leq 19$), the measured tangential poloidal magnetic field B_m ($1 \leq m \leq 38$), the measured poloidal flux and their time derivatives F_f and U_f respectively ($1 \leq f \leq 38$) and the measured total plasma current I_p (which is in fact redundant because it is obtained via B_m and Ampère's law). As the vessel is a conductor, the ohmic transformer induces the circulation of strong toroidal currents in its bulk. To account for this, we divide it into current filaments I_v ($1 \leq v \leq 38$) and treat it as a source of B-field. In the same way, we divide the inside of the vessel in a fixed grid of filaments I_x, where the grid is placed columns after columns in a column vector ($1 \leq x \leq 462$). All the parameters that have been defined here are not independent, but linked *linearly* by basic electromagnetic laws like Biot & Savart's law (we consider a quasi static case) for B_m and mutual induction law for F_f. In addition to this, an efficient constraint is given by the tension equation on the circuits formed by the vessel filaments:

$$0_v = R_{vv} I_v + M_{v_i v_j} \frac{d}{dt} I_v + M_{va} \frac{d}{dt} I_a + M_{vx} \frac{d}{dt} I_x \tag{1}$$

where R_{vv} is a diagonal matrix containing the resistance of each vessel filament and $M_{\alpha\beta}$ contains the mutual inductances between systems α and β. As the aim of this modelisation is to find a good fit (between measures and physical laws) for the different currents, one has to write a system of equations with the fitted values as unknown (noted with a "?") and to solve it in

a least square sense.

$$\begin{bmatrix} F_f \\ B_m \\ I_a \\ I_p \\ U_f \\ 0_v \end{bmatrix} \approx \begin{bmatrix} M_{fa} & M_{fv} & M_{fx} & 0_{fa} & 0_{fv} & 0_{fx} \\ B_{ma} & B_{mv} & B_{mx} & 0_{ma} & 0_{mv} & 0_{mx} \\ 1_{aa} & 0_{av} & 0_{ax} & 0_{aa} & 0_{av} & 0_{ax} \\ 0_{pa} & 0_{pv} & T_{px} & 0_{pa} & 0_{pv} & 0_{px} \\ 0_{fa} & 0_{fv} & 0_{fx} & M_{fa} & M_{fv} & M_{fx} \\ 0_{va} & R_{vv} & 0_{vx} & M_{va} & M_{vv} & M_{vx} \end{bmatrix} \cdot \begin{bmatrix} \hat{I}_a \\ \hat{I}_v \\ \hat{I}_x \\ \frac{d}{dt}\hat{I}_a \\ \frac{d}{dt}\hat{I}_v \\ \frac{d}{dt}\hat{I}_x \end{bmatrix} \tag{2}$$

The equation system (2) contains the whole knowledge that we have in our case. T_{px} is a line vector of ones. Note that the linking matrix depends only on the geometry of the experiment.

In the actual form of our system, a problem is encountered: there are more unknowns than equations because there are too many current filaments for the plasma and the vessel. Hence, if a least square approach has to be used, the number of unknowns has to be decreased.

3.1.1 Plasma current modelisation

To decrease the number of parameters describing the inner core of the vessel, the plasma filaments are replaced by a sum of pyramidal finite elements, labeled here by b ($1 \leq b \leq 15$). In this approach, each pyramidal element comprises many plasma filaments, giving them a weight proportional to their distance to the top of the pyramid. In the central zone of the vessel, the pyramidal elements overlap themselves in order to have a globally constant weight for each plasma filament. By this mean, the problem of edge conditions of the finite elements is passively solved. Mathematically, this is formulated in the following way:
Let us call r_i ($0 \leq i \leq 4$) and z_j ($0 \leq j \leq 6$) the coordinates of the corners of the elements. We write the amplitude of the finite element (i, j) ($1 \leq i \leq 3$ and $1 \leq j \leq 5$) at point (r_x, z_x) as

$$\begin{aligned} T_{xb} = &\left(\frac{r_x - r_{i-1}}{r_i - r_{i-1}}(r_{i-1} \leq r_x < r_i) + \frac{r_{i+1} - r_x}{r_{i+1} - r_i}(r_i \leq r_x < r_{i+1}) \right) \\ &\cdot \left(\frac{z_x - z_{j-1}}{z_j - z_{j-1}}(z_{j-1} \leq z_x < z_j) + \frac{z_{j+1} - z_x}{z_{j+1} - z_j}(z_j \leq z_x < z_{j+1}) \right) \end{aligned} \tag{3}$$

This gives the transformation matrix from the I_b currents (estimators of the plasma currents in each pyramidal element) to the I_x currents and also the transformation for the mutual inductances as follows:

$$I_x = T_{xb} I_b \tag{4}$$

$$M_{\alpha b} = M_{\alpha x} T_{xb} \tag{5}$$

where α is a free index.

An important variable in the present modelisation is the position of the center of gravity of the plasma current. It is defined as:

$$\begin{aligned} r_{CG} &= \frac{\sum_x r_x I_x}{\sum_x I_x} \\ z_{CG} &= \frac{\sum_x z_x I_x}{\sum_x I_x} \end{aligned} \tag{6}$$

This variable will be of crucial importance in the statistical treatment and the determination of the relevance of the magnetic field conditions. A typical time evolution of the center of gravity can be seen in figure 2.

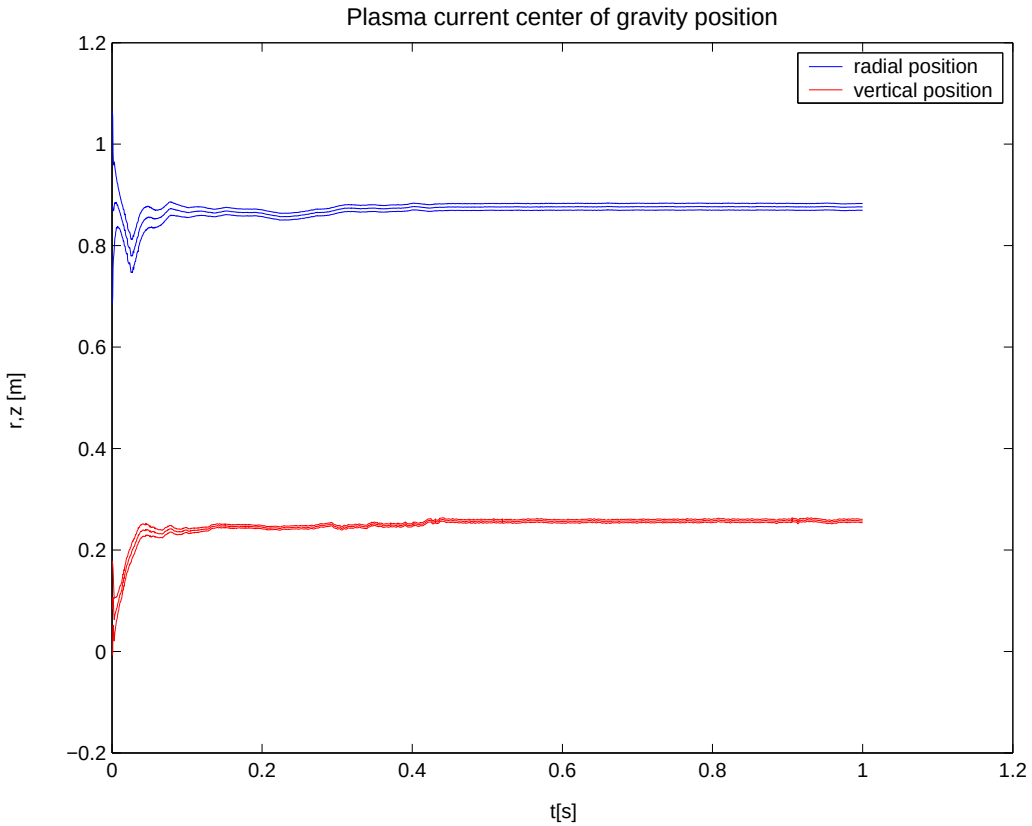

Figure 2: Calculated trajectory of the plasma current center of gravity in shot 10 000. The triplets are obtained by addition and subtraction of the time-dependent error (cf. sect. 3.4.2). The evolution is shown for $I_p \geq 4000\,\mathrm{A}$.

3.1.2 Vessel current modelisation

Having done the previous work, experience shows that it is not really necessary to decrease further more the number of unknowns. This section shows how this is yet possible using an eigenmodes representation method. The physical ground of this method is that the vessel current can be expressed as the sum of a finite number of currents with a characteristic geometric distribution (harmonics) and characteristic times of evolution. By decomposing the vessel current on such a basis, it is then possible to remove the eigenmodes with characteristic times smaller than the one of the experiment (set here as a multiple of the sampling frequency of the probes). In addition to this time-based argument, this selection also relies on the fact that these particular eigenmodes have a geometrical distribution that has a poor probability to be excited. Mathematically, the eigenmode approach is expressed as the diagonalization of an operator combining the resistance of the vessel filaments and their mutual inductances. The development can be summed up by the following expressions:

$$R_{vv} + M_{v_i v_j}\frac{d}{dt} =: T_{ve}(R_{ee} + M_{ee}\frac{d}{dt})T_{ev} \tag{7}$$

where

$$T_{ve} := R_{vv}^{1/2}\Gamma_{ve}R_{ee}^{-1/2} \tag{8}$$
$$T_{ev} := R_{ee}^{-1/2}\Gamma_{ev}R_{vv}^{1/2} \tag{9}$$

where Γ_{ve} is an orthogonal matrix defined by (7), R_{ee} is defined by the constraint that T_{ve} and T_{ev} must be inverse of each other and $M_{ee} := R_{ee}T_{ee}$.

Writing then $I_v = T_{ve}I_e$ and $M_{e\alpha} = T_{ev}M_{e\alpha}$, and multiplying the tension equation (1) to the left by T_{ev}, it yields:

$$0_e = (R_{ee} + M_{ee}\frac{d}{dt})I_e + \sum_\alpha M_{e\alpha}\frac{d}{dt}I_\alpha \tag{10}$$

Defining $M_{\alpha e} = M_{\alpha v}T_{ve}$, it is then possible to write the new equation system for the reduced number of parameters:

$$\begin{bmatrix} F_f \\ B_m \\ I_a \\ I_p \\ U_f \\ 0_e \end{bmatrix} \approx \begin{bmatrix} M_{fa} & M_{fe} & M_{fb} & 0_{fa} & 0_{fe} & 0_{fb} \\ B_{ma} & B_{me} & B_{mb} & 0_{ma} & 0_{me} & 0_{mb} \\ 1_{aa} & 0_{ae} & 0_{ab} & 0_{aa} & 0_{ae} & 0_{ab} \\ 0_{pa} & 0_{pe} & T_{pb} & 0_{pa} & 0_{pe} & 0_{pb} \\ 0_{fa} & 0_{fe} & 0_{fb} & M_{fa} & M_{fe} & M_{fb} \\ 0_{ea} & R_{ee} & 0_{eb} & M_{ea} & M_{ee} & M_{eb} \end{bmatrix} \cdot \begin{bmatrix} \hat{I}_a \\ \hat{I}_e \\ \hat{I}_b \\ \frac{d}{dt}\hat{I}_a \\ \frac{d}{dt}\hat{I}_e \\ \frac{d}{dt}\hat{I}_b \end{bmatrix} \tag{11}$$

Note that $T_{pb} = T_{px}T_{xb}$.

3.2 Time evolution

The problem that arises here is that as we do not solve the system analytically, we cannot treat the unknowns and their derivatives as independent variables. If we do so, that is if we apply directly a least square fitting to the system (11), we observe a strong deviation between the fitted derivatives and the derivatives that we can compute *a posteriori* using the fitted currents. The reason for this behaviour is that the fitting is done independently for each increment of time. Ideally, the best answer to this problem would be to introduce the derivation inside the linking matrix and to solve the system for all the currents and all the times at once. This would represent a least square fit of about 500 000 parameters at the same time, which is obviously not achievable. The second best answer (to our eyes) is to put a constraint between the fitted derivatives and the derivatives of the fitted currents, using an iterative process. The new system of equations is then:

$$\begin{bmatrix} F_f \\ B_m \\ I_a \\ I_p \\ U_f \\ 0_e \\ \frac{d}{dt}I_a \\ \frac{d}{dt}I_e \\ \frac{d}{dt}I_b \end{bmatrix} \approx \begin{bmatrix} M_{fa} & M_{fe} & M_{fb} & 0_{fa} & 0_{fe} & 0_{fb} \\ B_{ma} & B_{me} & B_{mb} & 0_{ma} & 0_{me} & 0_{mb} \\ 1_{aa} & 0_{ae} & 0_{ab} & 0_{aa} & 0_{ae} & 0_{ab} \\ 0_{pa} & 0_{pe} & T_{pb} & 0_{pa} & 0_{pe} & 0_{pb} \\ 0_{fa} & 0_{fe} & 0_{fb} & M_{fa} & M_{fe} & M_{fb} \\ 0_{ea} & R_{ee} & 0_{eb} & M_{ea} & M_{ee} & M_{eb} \\ 0_{aa} & 0_{ae} & 0_{ab} & 1_{aa} & 0_{ae} & 0_{ab} \\ 0_{ea} & 0_{ee} & 0_{eb} & 0_{ea} & 1_{ee} & 0_{eb} \\ 0_{ba} & 0_{be} & 0_{bb} & 0_{ba} & 0_{be} & 1_{bb} \end{bmatrix} \cdot \begin{bmatrix} \hat{I}_a \\ \hat{I}_e \\ \hat{I}_b \\ \frac{d}{dt}\hat{I}_a \\ \frac{d}{dt}\hat{I}_e \\ \frac{d}{dt}\hat{I}_b \end{bmatrix} \tag{12}$$

The iteration process goes as follows: the input is initiated by setting the derivatives equal to zero. The system is then solved and the fitted currents are used to generate the next input derivatives. This method converges quite fast but the convergence is rather towards a stable difference between the two kinds of derivatives, than towards a null difference. The exit criteria relies consequently on the difference of errors between two iterations.

Despite the idea is good, we encounter a lot of problems while trying to apply it directly. For example, there is still a quite big difference between the fitted derivatives and the recomputed ones (appearing as noise on the latter). In addition, the choice of free parameters (see below) has a strong impact on the generic character of the program: i.e. the program can give coherent and relevant results in a certain shot and completely false ones in another. The solution resides in the fact that the derivatives of the fitted currents are strongly noised. This means that the fitted currents probably oscillate around a smooth curve and that taking a direct derivation of them is not significative. The application inside the iteration process of a low-pass

filter on the fitted currents and on their derivatives has appeared to be very efficient in solving the said problems. In addition, it increases the speed of convergence of the iteration loop.

3.2.1 Breakdown time

In the present form of our equation system, there is a possibility that the least square solving results in a solution giving non null plasma currents while it is pretty sure that the plasma is still not formed (e.g. solutions with some currents going in one direction and others in the other, thus cancelling themselves globally). To avoid this non physical behaviour, we can use the knowledge of the total plasma current to give an additional constraint for the resolution of our equation system. The trick is to select all the times when the plasma has a high probability of existing and to solve (12) for these times only. For all the remaining times, it is only a subsystem (obtained by removal of plasma filaments occurrences) that is solved. The weakness of this process is that there is an absolute choice that has to be made on the existence of the plasma. Unfortunately, it seems quite hard to define a parameter for this choice that could be implemented in the equation system and fitted simultaneously to the others in order to optimize the breakdown time value t_0.

A first attempt to find t_0 consisted in applying a threshold value test on the I_p measurements, the retained value for this test being of 4000 A. The standard deviation on the measurement of the plasma current being of 1000 A, this corresponded in fact to a probability of 0.95 to be in the presence of a plasma. Actually, according to the order of size of the other currents in presence at that time (20 kA for the ohmic coils, and above all a total vessel current of the order of 100 kA), the magnetic influence of the plasma current in its beginning is weak and the absolute value of I_{p_0} seemed therefore not to be so important. As far as the error on breakdown time is concerned, it can anyway only be of some time increments as the total plasma current increases extremely fast due to the very low resistivity of the plasma.

However, the aim of this project is to characterize the fine magnetic behaviour of the system around the breakdown time. Thus it is crucial to know precisely the latter in order to have a relevant analysis. In consequence, the approximations taken above, which are absolutely sensible for the global study of the system, could turn out to be very damaging in our case.

The final applied method for determining t_0 is to use the sign of the time derivative of I_p as the argument of a test. The latter consists in saying that if there is a sequence of a certain length during which $\frac{d}{dt}I_p$ is always bigger than zero, then breakdown occurs at its beginning. The validity of this algorithm

relies on the fact that the increase of plasma current is so steep that there should be a null probability to have an I_p value smaller than the previous one during breakdown. However, noise on the I_p measurements can drive to this kind of bad situation. The solution consists thus to firstly use a low pass filter on I_p to reduce this noise, and then to define a test loop with a decreasing test level (i.e. decreasing number of consecutive positive time derivatives) if a comparison test with the threshold value test gives a false result. The latter simply forces the t_0 value given by the time derivative test to be smaller than the one given by the threshold value test and not too distant from it. Note also that the threshold value test is kept for determining the plasma vanishing time. Application of this new method has revealed to be very reliable, allowing an important increase of accuracy on t_0. It also allows us to recalibrate the I_p current around the breakdown time. This is done by building a linear drift function based on a local mean of I_p at the beginning of the measurements and a second one just before the breakdown. This drift function is then subtracted from I_p until it reaches 20 kA, thus limiting the impact of this correction under the uncertainty on I_p and improving considerably the behaviour of the I_b's around t_0.

3.3 Equations weighting

Our model, in the present state, is still uncomplete because the least square fit generally compares absolute differences between the fitted values and the measured ones. This means that we have to normalize the different physical values that we use in such a way that each equation of the system deals with numbers of the same order of size. To do that, we simply have to multiply to the left each member of the equation system by a diagonal matrix of weights W. This corresponds to:

$$y \approx A \cdot x \qquad \rightarrow \qquad Wy \approx WA \cdot x \tag{13}$$

where y, A, x represent the three main terms of (12). A very good way to find the values that have to be used for the normalization is to have a look at the parameter of the least square fit, namely χ^2. For our final system, it is expressed as:

$$\chi^2 = \sum_i w_i^2 (y_i - (A \cdot x)_i)^2 \tag{14}$$

When the least square fit is realized, the χ^2 is minimum and expressed as:

$$\chi^2_{min} = \sum_i w_i^2 \underbrace{(y_i - (A \cdot \hat{x})_i)^2}_{\sim \sigma^2_{y_i}} \tag{15}$$

As noted, the deviation should be of the order of the variance $\sigma_{y_i}^2$ for each measured value. Therefore, we only have to set the w_i^2 as being equal to the inverse of the variances in order to treat the equations uniformly. Note that the method proposed here does not correspond exactly to normalizing the equations with respect to the size of the numbers they are dealing with. Imagine for example that the standard deviation of a value is two order of size smaller than the value itself. Then, the corresponding weight would be 100 times bigger than the one that should be used in a pure normalization case. Thus, our method not only normalizes the equations but also account for the quality of the measurements. By this mean, we also obtain a very good test parameter for our model. Let us call this parameter p_{test} and define it by:

$$p_{test} := \frac{\chi^2_{min}}{\sum_i w_i^2 \sigma_{y_i}^2} \tag{16}$$

p_{test} is a function of time but is practically used in its average around the breakdown time. If our model is good, then p_{test} should be in the neighborhood of 1. If it is much bigger than 1, then there are two possible explanations: either the experimental deviations are underestimated, or the model does not fit to reality. In the second case, some freedom is given by the input values on which we do not have any experimental deviation, like for the vessel tension equation and for the derivative constraints. Individual tests for each equation can also be constructed in the same way. For example, one of our tests consists in normalizing each deviation in function of time by dividing it by the corresponding given deviation. The result of this normalization is then plotted under the shape of a color map, giving thus a very good indication on the obtained fit (see fig. 3). It allows for instance to look for non-typical measurements that can be treated separately later on (removed from the set of equations).

Another useful quality estimator is given by a group version of p_{test}, where the summation for the χ^2 and the normalization denominator only bears on each group of equations individually. Although the results of such an estimation is not as compact as p_{test}, it removes the unseen phenomenons of compensation that can occur when giving a very big deviation on the wrong equations. Results of such an analysis can be seen in figure 4.

The method used for the allocation of the weights is the following. The program is firstly run using a set of weights based on the experimental uncertainties for the "experimental" group of equations, an arbitrary weight of 1 on the tension equation and a weight zero for all the other constraints. Then, the individual χ^2 tests are analyzed and the program is run again with new weights based on this analysis. This process is repeated until the tests appear

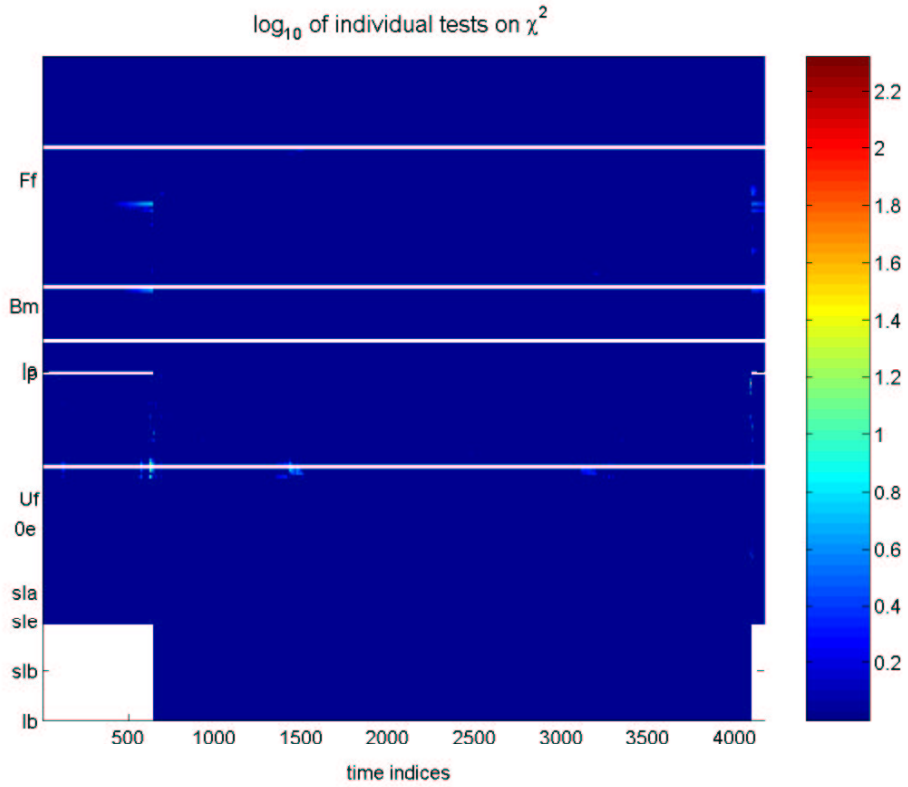

Figure 3: Individual tests on deviations in function of time for the shot 10 000 with an eigenmode representation. The deep blue zones indicate that the obtained deviation is smaller than the attributed one. The other zones correspond to the log_{10} of the proportionality factor. The white parts reflect the removal of the concerned equations in the calculation (see sect. 3.5).

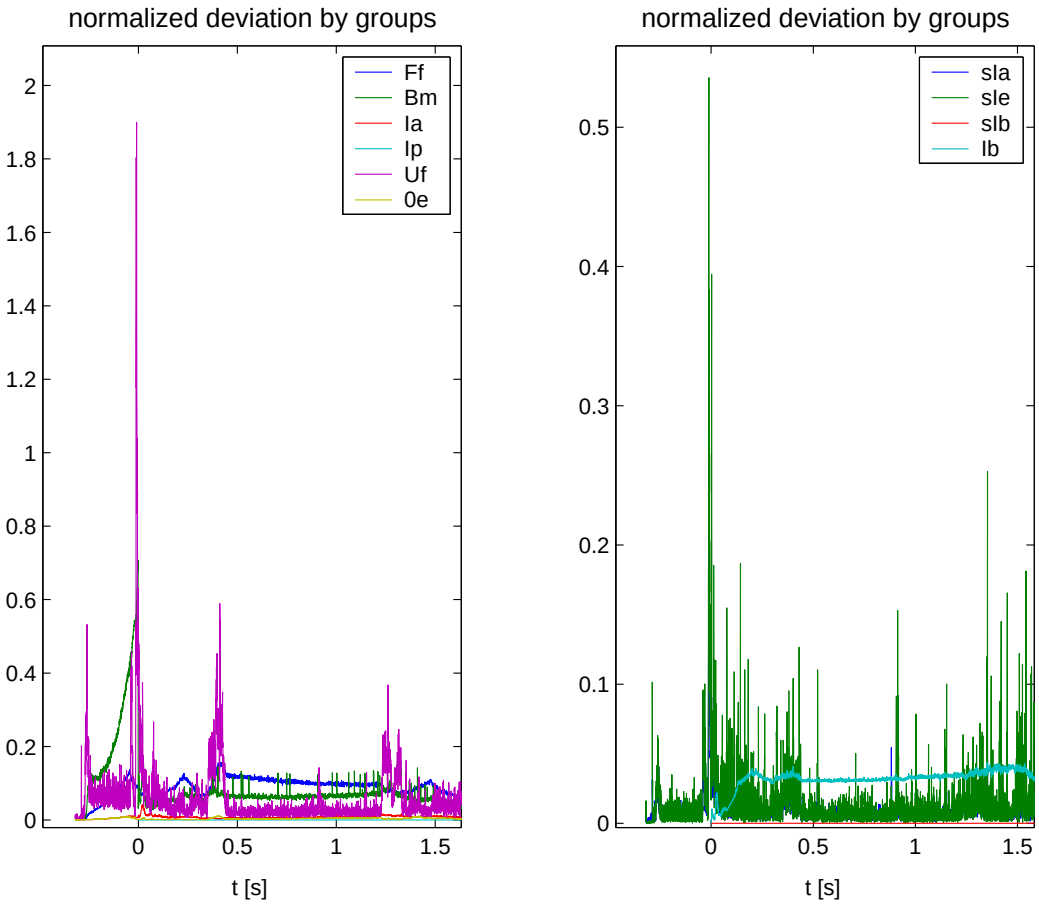

Figure 4: Normalized deviations by groups using an eigenmode representation (shot 10 000). An explanation for the I_b deviation on the RHS can be found in sect. 3.5.

to be just passed. The best compromise is finally kept for the first part of the set of weights. By this way, we can assure a maximum of accuracy on the most relevant equations. Having done this, an arbitrary set of weights is given for the other constraints and once again the convergence process based on the obtained deviations and on the set of tests is repeated.

As the sampling frequency f_e is not always the same in the different shots, the accuracy on the currents derivative constraints can change between some of them. To account for that, we have to consider what effects result from a change in f_e. There are two antagonist things happening if the latter increases. The first one is that the time increment between two points is smaller, which means an increase of accuracy going as f_e^2 from the definition of the derivative point of view. The second one is that there is noise on the data that we use to calculate the derivatives, such that approaching one point from the following one results in an increase of uncertainty going as f_e from the geometric construction of the derivative point of view. Altogether, the accuracy on these constraints goes as f_e.

The last point concerning the weights is their distribution among the groups of equations. Until now, the weights are independent of the number of equations for each group. In this conception, each measure or constraint has the same effect (before weighting) whatever the group. If one considers that the global effect of each group should be equal (before weighting), then one has to divide the weights by the number of equation k_i in each group. This ends to:

$$w_i := \frac{1}{\sigma_{y_i} k_i} \tag{17}$$

A more sophisticated approach consists in making a compromise between these two conceptions by dividing by $\ln(1 + k_i)$ (for example) instead of k_i. By this way, the impact of a group increases logarithmically with the number of equations it contains.

3.4 Errors treatment

The knowledge of the error propagation throughout our work is crucial to assess its usefulness and the relevance of the conclusions it will bring. Therefore, a strong emphasis has been laid on this part of the job. The basis of this study is the calculation of the covariance matrix of the fitted currents and of their derivatives.

3.4.1 Fitted parameters covariance matrix

The first step in this calculation is to express literally the values of the fitted parameters obtained by the least square fit method. This is simply done by minimalizing the χ^2 with respect to x_i's. One obtains (without the weights):

$$\hat{x} = (A^\dagger A)^{-1} A^\dagger y \tag{18}$$

The weights can be simply integrated in (18) by multiplying each A and y by W (before applying the $\dagger$ operators). Note that A is not directly invertible as it is not a squared matrix. By definition, the covariance matrix $\sigma_{x_i x_j}$ of x is given by:

$$\sigma_{x_i x_j} = \boldsymbol{E}\{(x - \bar{x}) \cdot (x - \bar{x})^\dagger\} \tag{19}$$

where $\boldsymbol{E}$ is the expectation value symbol. The formalism used here implies (theoretically) the repetition of the same shot a big number of times giving $\bar{x}$ as the average solution and using x as the random variable. Writing $\bar{x}$ as the solution corresponding to the average input values $\bar{y}$ and y as the random input variable corresponding to x, we have through (18) (without the weights):

$$\sigma_{x_i x_j} = \boldsymbol{E}\{[(A^\dagger A)^{-1} A^\dagger y - (A^\dagger A)^{-1} A^\dagger \bar{y}] \cdot [(A^\dagger A)^{-1} A^\dagger y - (A^\dagger A)^{-1} A^\dagger \bar{y}]^\dagger\} \tag{20}$$

Using the properties of the $\dagger$-operator and the linearity of the expectation value gives then:

$$\sigma_{x_i x_j} = (A^\dagger A)^{-1} A^\dagger \ \boldsymbol{E}\{(y - \bar{y})(y - \bar{y})^\dagger\} \ A (A^\dagger A)^{-1} \tag{21}$$

$$\sigma_{x_i x_j} = (A^\dagger A)^{-1} A^\dagger \ \sigma_{yy} \ A (A^\dagger A)^{-1} \tag{22}$$

where σ_{yy} is the covariance matrix of y. It is a diagonal matrix since measurements are taken independently. Note that $(\sigma_{yy})_{ii} := \sigma_{y_i}^2$. Integrating the weights into the formula, it yields:

$$\sigma_{x_i x_j} = (A^\dagger W^2 A)^{-1} A^\dagger W^2 \ \sigma_{yy} \ W^2 A (A^\dagger W^2 A)^{-1} \tag{23}$$

We can see in this formula that the covariance matrix is (nearly) independent of the shot itself, but that it depends on the geometry of the experiment through A, on the weighting of the equations, on the intrinsic errors of the measurements and on the presence or absence of plasma. The shot dependence relies on the used sampling frequency, which determines the number of eigenmodes and the standard deviation of the constraints on the currents derivatives. A process of optimization of the fit (described in sect. 3.5) also tends to decrease partly this generic feature. Nevertheless, the covariance

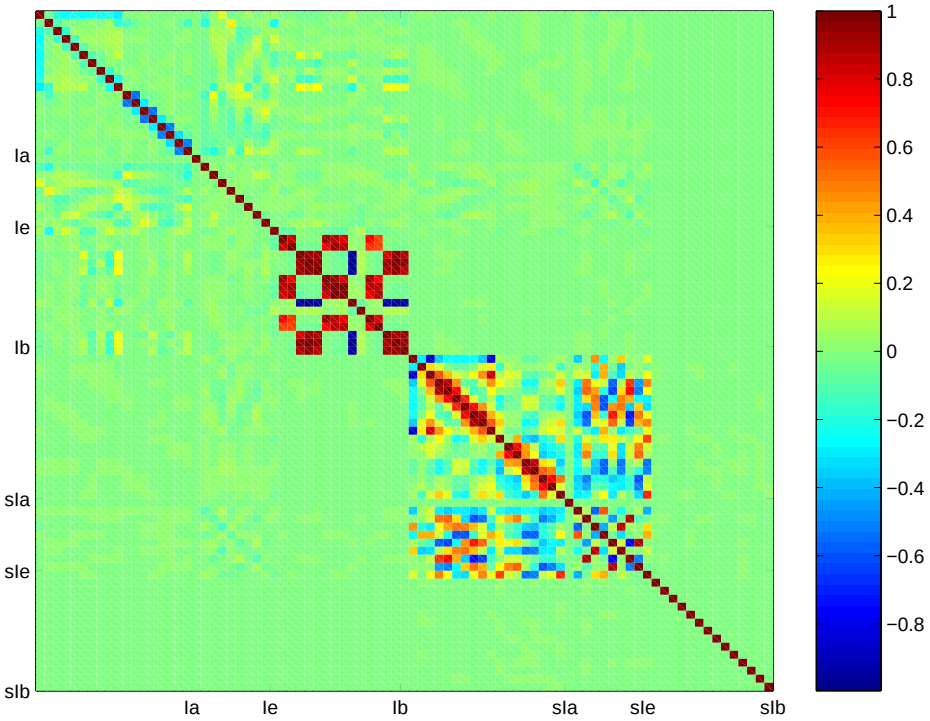

Figure 5: Relative covariance matrix for the shot 10 000 in the case with plasma, using an eigenmode representation. The matrix is obtained by dividing each element of the covariance matrix by the product of the standard deviations of both corresponding fitted parameters.

matrix has a strong generic character and is hence a good source of information for the quality of the model. An example of the relative covariance matrix for the case with plasma is shown in figure 5.

The correlation between the fitted parameters indicated by the covariance matrix is normal to a certain extent, as it comes from the constraint of minimization of χ^2. However, if the covariances between the fitted parameters are big relative to the variance of the parameters themselves, this indicates that the modelisation can bring non physical behaviours in order to achieve the minimization. In such cases, that can mean that the choice of parameters is not good. Despite all the information contained in it, the covariance matrix, as an analysis tool, is much more useful to compare the quality of different configurations of the model than to find the sources of problems.

The direct implementation of the formula (23) in *Matlab* leads to error messages because of remaining normalization problems in the matrix A. To avoid this problem, the *backslash* function can be used with another approach of the covariance calculation relying on:

$$\mathrm{cov}(Wy) = \mathrm{cov}(WAx) \tag{24}$$

Once again, linearity properties are used, in addition to the symmetry of the covariance matrix, to give:

$$\sigma_{x_i x_j} = (WA)\backslash[(WA)\backslash(W\sigma_{yy}W)]^\dagger \tag{25}$$

The use of this formulation gives results equal to the previous ones, to computer's accuracy.

3.4.2 Errors calculation

Having done the calculation of the currents covariance matrix, it is then very simple to evaluate the errors on the different interesting outputs of our model. For the currents and their derivatives, one just have to take the diagonal of $\sigma_{x_i x_j}$ to obtain their variances. For any other variable v depending on I's or on $\frac{d}{dt}I$'s, the general rule of error propagation (26) is simply applied.

$$\sigma_{v_i v_j} = \nabla_{x'} v \cdot \sigma_{x'_i x'_j} \cdot \nabla_{x'} v^\dagger \tag{26}$$

where x' is a subpart of x. Generally, the linearity of v with respect to x greatly simplifies the calculation, as the Jacobian matrix is then equal to the transformation matrix between v and x (e.g. in the cases of the magnetic fields and of the circular tensions). As far as the center of gravity of the plasma current is concerned, the calculation is simplified by saying that the

error only bears on the current distribution inside the plasma itself, but not on the grid points position neither on the total plasma current. One obtains:

$$\begin{aligned} \sigma^2_{r_{CG}} &= \frac{1}{\sum_x I_x}(r_1,\ldots,r_{n_x})\ \sigma_{I_{x,i}I_{x,j}} \begin{pmatrix} r_1 \\ \vdots \\ r_{n_x} \end{pmatrix} \\ \sigma^2_{z_{CG}} &= \frac{1}{\sum_x I_x}(z_1,\ldots,z_{n_x})\ \sigma_{I_{x,i}I_{x,j}} \begin{pmatrix} z_1 \\ \vdots \\ z_{n_x} \end{pmatrix} \end{aligned} \tag{27}$$

As the given formulation contains a division by the total plasma current, the above deviations are not usable as they appear here for the times of low plasma current. Therefore, the error has been further approximated in the breakdown phase as being the time average of the calculated error. At this point, one has to point out the fact that the given formulation for the error gives information on the propagation of the error inside the model, but not on the model itself. That means that the loss of resolution by the discretization of the core of the vessel and further more by the use of finite elements is not taken into account in (27). Pyramidal finite elements are quite good from this point of view because their overlap increases the resolution of the method. Thus, we can say that we have a resolution on the center of gravity of approximately a quarter of a pyramidal element.

Equation (26) is also used in order to determine the errors on the magnetic field. In this case, the error map on the cross section is independent of time because the magnetic field is a simple linear combination of the fitted currents. Figures 6 and 7 show the typical behaviour of the error across the cross section. Note that the error on B when the plasma is present (fig. 7) does not contain the terms due to the plasma itself. This is due to the fact that we are firstly interested in the controllability that we have on the weak B-field, and thus in the impact of the coils and of the vessel. We can observe that the error is surprisingly smaller in the center than close to the probes. This is a consequence of the least square solving, which tends to interpolate the different measurements. As the central zone of the cross section is covered by a bigger number of probes than the peripheral one, the level of information on it is higher.

3.5 Free parameters discussion

Despite all the efforts made to reduce the number of arbitrary parameters used in the model, there is still a certain number of them that we cannot get

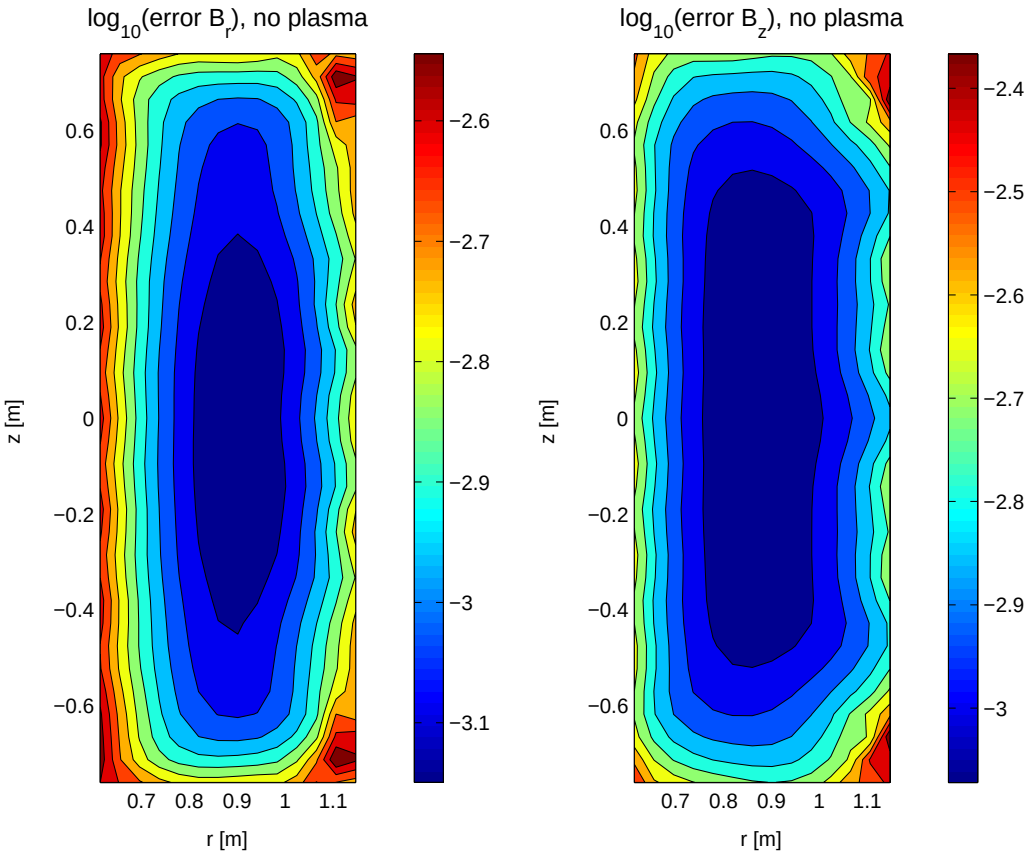

Figure 6: $\log_{10}$ of the errors on B_r and B_z for the shot 25 016. Plasma is not present and the eigenmode representation is used. The magnetic field is in tesla.

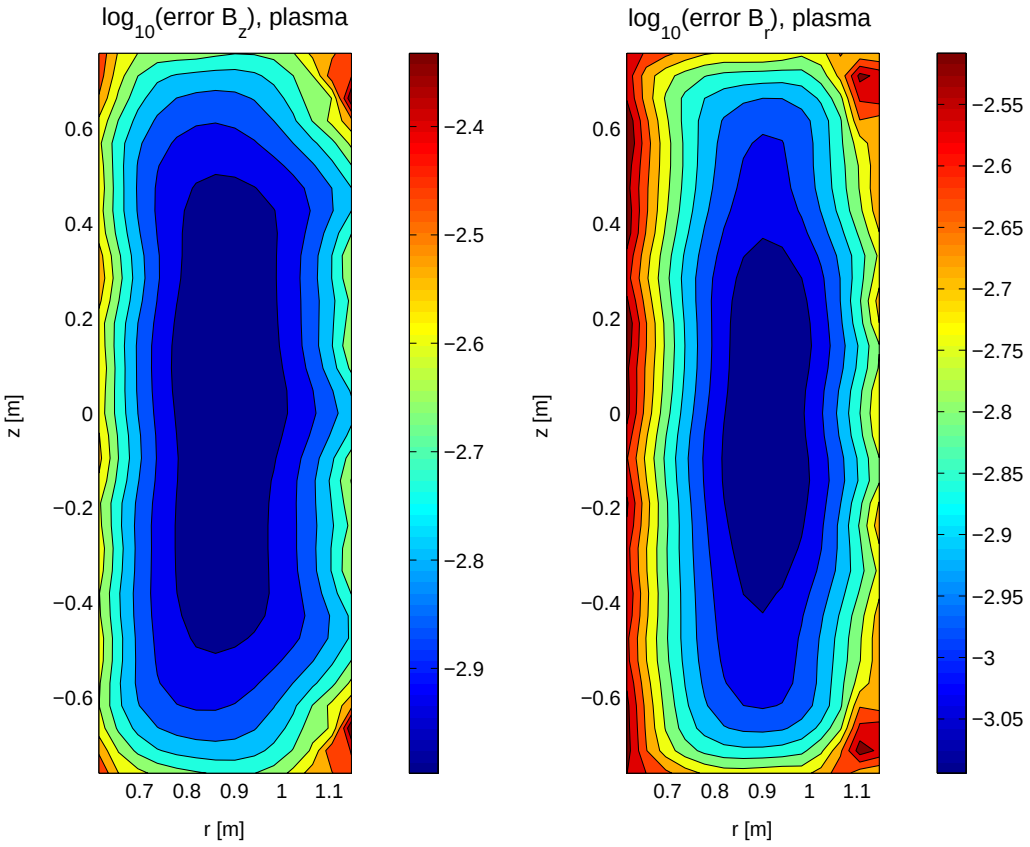

Figure 7: $\log_{10}$ of the errors on B_r and B_z for the shot 25 016. Plasma is present but not used as an explicit source of error, and the eigenmode representation is used. The magnetic field is in tesla.

rid of. We give here their list, comprising the eventual physical grounds for the choice of their values. Generally, a serious problem encountered during the optimization of these parameters is that above a certain optimization level, the behaviour of the solution is not generic on the different shots.

3.5.1 Number of plasma finite elements, further enhancements

In determining the optimal number n_b of pyramidal finite elements for describing the inner core of the vessel, we have to play between two antagonist arguments. If n_b is too big, the least square fit tends to give non physical results, while if it is too small the resolution on the plasma current center of gravity becomes very poor. To avoid partly this antagonism, a subtle process has been developed. It is composed of two complementary arguments. The first one consists in adding a set of constraints on the I_b's into the equation system. Their expression is simply:

$$0 = I_b \tag{28}$$

Despite this look rather strange and non physical, the idea is that their impact on the least square solving is given by a minimization of the sum of the I_b^2's. If the I_p equation is assured to be well fitted, this leads to a preference for a solution where all the I_b's have the same sign, improving thus its reliability. The play consists then in choosing a good weight for this constraint, so that it remains effective but harmless. The trick is to consider the case where all the plasma is in a unique pyramidal element and to calculate the corresponding value for the concerned I_b (which is *not* simply equal to I_p because of T_{xb}). Then, the variance on the constraint is set to be equal to this value, as equation (28) is correct only within the uncertainty interval defined by the maximum of I_b. Direct application of this argument leads to an important improvement of the behaviour of the solution, but not sufficient for choices like $n_b = 15$, which is a very optimistic (and, at first sight, close to utopian) choice.

The complementary argument consists in using an iterative loop based on two tests on the behaviour of the I_b's, in order to keep only those that are relevant to our model. Both tests rely on the fact that the plasma position is nearly constant throughout the shot. Consequently, if an I_b is too much or too long in the wrong direction, then it can be considered that there is no plasma at all in the corresponding pyramidal element. The first test filters out the I_b's that have a time integral with a sign opposite to the I_p's sign. The second test filters out the I_b's that have the wrong sign during a too long time, and use a test level increasing with the number of iterations but stopping at 87.5% of correct sign. By "filter out", we mean that the constraint weights of the I_b's

that do not pass the tests are set to a high value while their corresponding variances are set to zero. By this mean, the least square solving forces the bad I_b's to zero and still applies the first argument for the others. The level of the second test has been chosen to increase between iterations because of the strong correlation between the I_b's. One has effectively to start with a low test level in order to eliminate only the relevant I_b's. After each iteration, the behaviour becomes more and more stable and it is then possible to increase the test level without risking to remove physically existent I_b's (see fig. 8). The only problem in our reasoning is that pyramidal elements containing the plasma only in its initial phase of drift, but not later on, are probably removed. Nevertheless, we can assume that the drift distance must be smaller than, or near to, the size of a finite element, and we can also profit of the overlap that occurs in their construction. This is in fact one of the reasons why we have not taken more than 15 elements up to now. A possibility for partly solving this problem would consist in decreasing the time interval of the solution to the time limit given by the constraint $I_p \leq 15\,\mathrm{kA}$ for example. Information on what happens after this threshold value would then be lost, but the solution would be much finer around the interesting times. It would also allow the application of the model for the shots where the plasma has been intentionally moved across the cross-section.

3.5.2 Number of eigenmodes

As described in sect. 3.1.2, the number of parameters describing the vessel currents can be reduced by using an eigenmodes representation. The questions arising then are how many of them must be taken and what is the influence of this choice on the solution. The first step of the reasoning is clearly to remove all the modes with characteristic times smaller than a multiple of the sampling time. Further than that, tests have shown that the effects of that choice on the magnetic field error or on the center of gravity error are negligible. The only observable effects have been small changes on p_{test} and the quality of the convergence of the method that increases for the choice of a bigger multiple. The final choice has thus been of $t_{charac} \geq 4 \cdot \frac{1}{f_e}$.

Another question is to know wether these eigenmodes have to be taken or not. In the present state, the equation system has a number of parameters sufficiently small to allow the use of the complete vessel model. If we do so, the accuracy on the magnetic field is appreciably increased. The covariance matrix also contains structures corresponding to the spatial distribution of the vessel segments. It shows yet a quite weak correlation between them (see fig. 9). It is however hard to determine if this correlation is smaller than the one of the eigenmodes, due to the geometrical extension of the latter. In

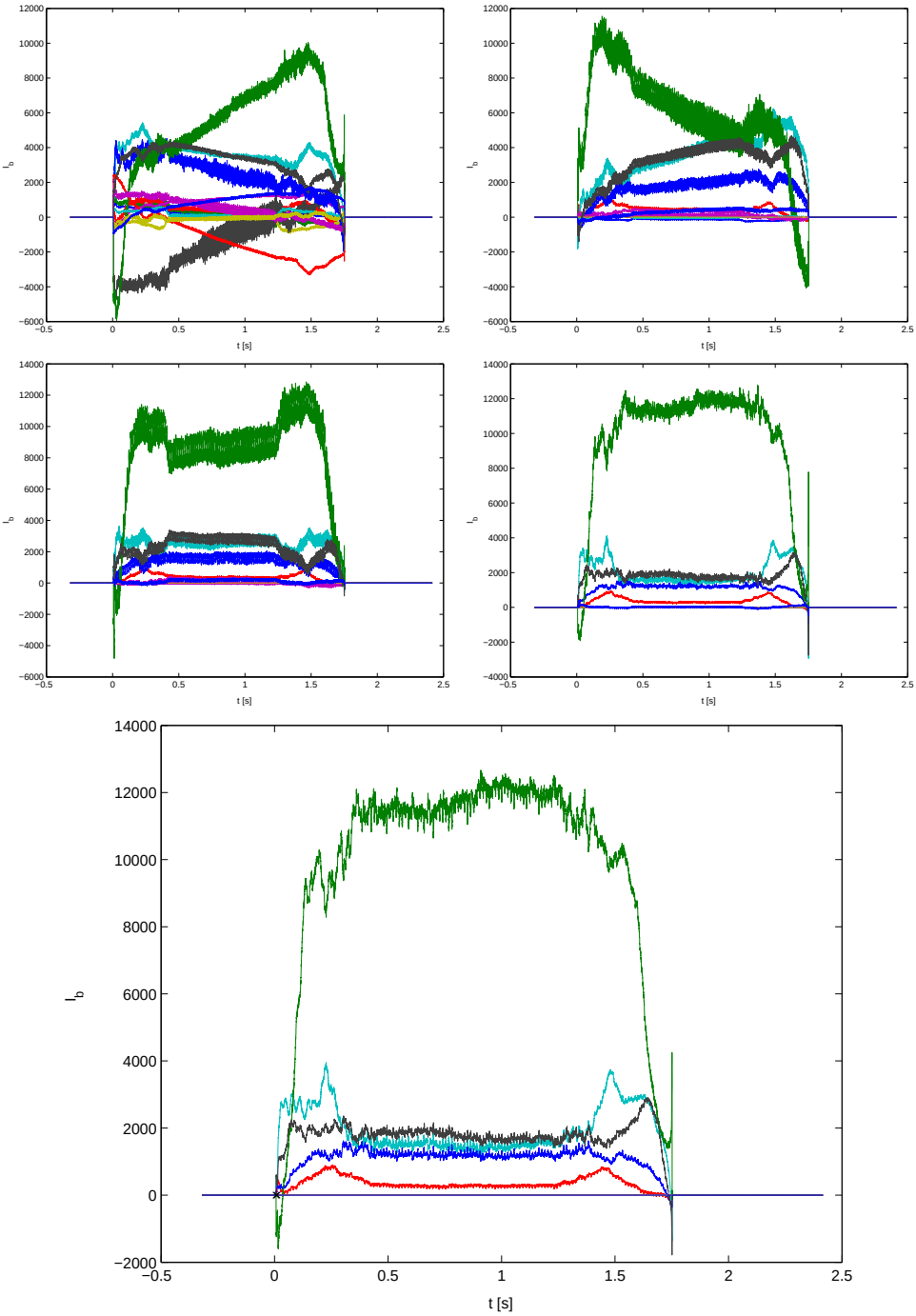

Figure 8: Plot of the I_b's along the iterative process in the shot 25 016, using an eigenmode representation. Bad solutions are successively set to zero. The last plot gives the retained solution.

the magnetic field reconstruction process, both options have proved to give similar results, allowing us to confirm the validity of our eigenmode method. When looking at the fitting of the model concerning the tension on the flux loops, it is observed that the segment representation leads to a much better fit (see fig. 10). The difference is so striking that we have decided to give another set of weights in this representation, getting thus a more accurate solution. The only negative aspect of using directly the vessel segments seems so to be the bigger amount of data that has to be stored and used in the calculations.

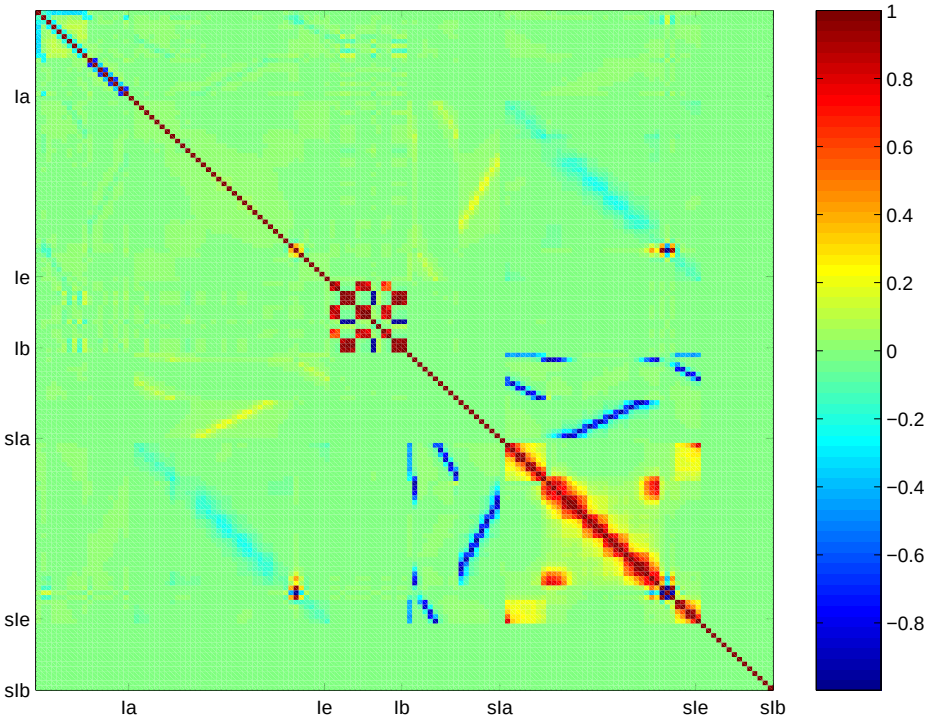

Figure 9: Relative covariance matrix for the shot 10 000 in the case with plasma, using a vessel segment representation. Compare with fig. 5.

3.5.3 Weights

The question of equation weighting is extensively treated in sect. 3.3. We will add here some considerations about the effects and problems that are met when the given arguments are used practically.

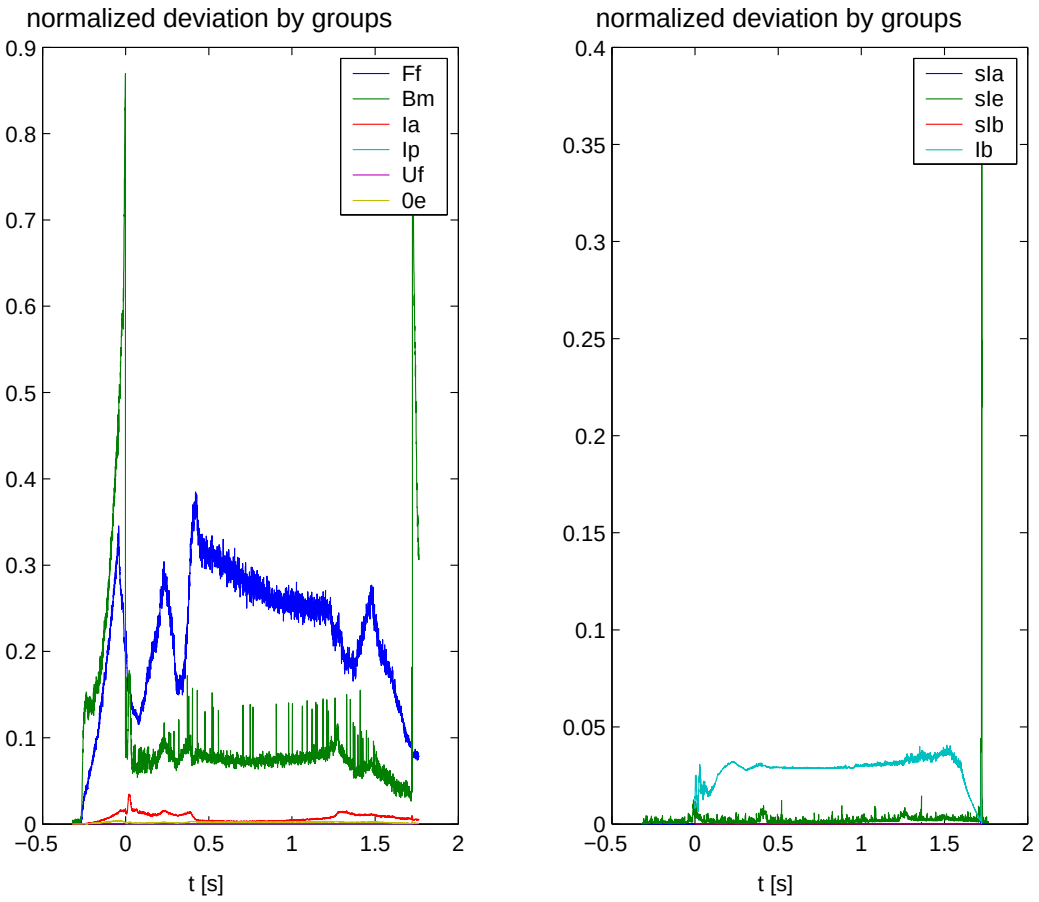

Figure 10: Normalized deviations by groups using a vessel segment representation (shot 10 000).

In the model, when a logarithmic increase of importance of the groups of equations with respect to their size is applied, many positive tendencies are observed. The main advantage is a much better fit of the model shown by p_{test}, which tends to decrease sometimes drastically. Therefore, this approach has been kept.

Another consideration about the weights is the fact that the optimal set of weights for a certain shot (i.e. giving a good fit with an error staying as low as possible), will generally not be good for another shot. The only way to obtain a generic weighting is to increase the error on the measurements, thus reducing the level of information that we can gain through our work. Solving this problem would require a kind of global iterative process finding automatically an approximation of the best weights for each shots. Although this does not seem impossible, it would take quite a long time to assure the stability and the physical relevance of such a process. We have thus adopted another way to manage with this situation, which is probably not as powerful as the given idea, but which is easy to apply and which gives very satisfying results. It consists in solving the equation system twice, the first time with all the available equations and the second time with a reduced number of equations where all the measurements that really do not fit with the solution are removed (thus eliminating the possibly defective probes, see fig. 3). The test is constructed as follows: for each measurement, the square of the deviation with respect to the fit is divided by the variance attributed to its group. Then, the obtained factors are summed along the time coordinate. We obtain thus a factor for each "experimental" equation. As the equations inside a group are treated uniformly, we can apply a statistical test on the obtained factors. It consists in removing all the equations inside a group that have a final factor bigger than the mean plus three times the standard deviation of all the factors of the group. Despite the high increase of robustness obtained by our method, the question of knowing wether the global treatment of the badly fitted measurements is correct with respect to the impact of each measurement on the fit of the others is still open. Another possibility would be to remove iteratively only the worst measurement in order to see the benefit on the rest of the fit, and to stop the process when the statistical test is passed for all the measurements. Despite it could lead to better results, this option would imply a bigger computational cost and would probably not seriously change the results. Anyway, experience has shown that the adopted method eliminates, in a very stable way, only a small number of measurements, and has proved thus to be appropriate.

The combination of the iterative processes for the weights and the plasma currents goes as follows. The first solution obtained with the complete set of plasma filaments can be considered as unstable because of the high number

of filaments that are used. Therefore, it is not advised to use it in order to determine the badly fitted measurements. The complete process that has been applied consists hence in firstly running the complete solver, testing and removing the worst I_b's (but keeping all the measurements), then running it a second time, testing and removing the inappropriate measurements and I_b's, and running it at least a third time to take the last corrections into account. The termination test relies on the absence of new corrections on the set of weights.

Another enhancement of the model has been to define two different sets of weights and variances for the cases of existence or non existence of the plasma. Initially due to a mistake in the code, this differentiation is nevertheless useful. In fact, the first observation that we can do when analyzing the normalized deviation by groups in function of time, is that it tends to follow the curve of plasma current. This shows that the plasma implies a noise on the measurement and that it is justified to change the variances during the time of plasma existence. The second observation is that the repartition of deviations is not symmetric around t_0 and by dividing the set of weights into two, we can have a finer adjustment of the model. The last point is that we can now set a null weight on the I_p equation before t_0, thus removing the artificial contribution of I_p on p_{test}. However, one has to chose two sets of weights that are not two much far from one another because otherwise the filtering on the currents would not be sufficient to remove the discontinuity between the cases with or without plasma.

The final set of standard deviations is given in table 1. There are four columns to account for the differences between the cases with or without plasma and depending on which representation of the vessel has been used. The corresponding weights are easily calculated by inversion of the deviation, and division by the size factor of the concerned group of equations. When the deviation is set to zero, the weight is also set to zero.

Input	Deviation				Units
	Eigenmodes		Segments		
	P	Np	P	Np	
F_f	10^{-2}	10^{-2}	$6{\cdot}10^{-3}$	$6{\cdot}10^{-3}$	wb
B_m	$5{\cdot}10^{-3}$	$4{\cdot}10^{-3}$	$5{\cdot}10^{-3}$	$4{\cdot}10^{-3}$	T
I_a	10^2	10^2	10^2	10^2	A
I_p	$5{\cdot}10^2$	0	$5{\cdot}10^2$	0	A
U_f	$5{\cdot}10^{-2}$	$5{\cdot}10^{-2}$	10^{-2}	10^{-2}	V
0_e	0.2	0.2	0.2	0.2	V
$\frac{d}{dt}I_a$	$T_e \cdot 10^8$	$T_e \cdot 10^8$	$2T_e \cdot 10^7$	$2T_e \cdot 10^7$	A/s
$\frac{d}{dt}I_e$	$T_e \cdot 10^{10}$	$T_e \cdot 10^{10}$	$2T_e \cdot 10^9$	$2T_e \cdot 10^9$	A/s
$\frac{d}{dt}I_b$	$T_e \cdot 10^6$	0	$2T_e \cdot 10^5$	0	A/s
I_b	$\frac{I_{p,max}}{T_{pb}(1)}$	0	$\frac{I_{p,max}}{T_{pb}(1)}$	0	A

Table 1: Standard deviations for each group of equations. T_e is the sampling period (e.g. 0.5 ms for the shot 10 000 and 0.2 ms for the shot 25 016). P or Np correspond to the presence or absence of plasma respectively.

4 Statistical analysis tools

The description of the construction of the general model having been done, we can now pass to the development of the tests and parameters that will be used for the statistical analysis. As said in section 2.2, the parameters of interest for our work are the magnetic field minima and their properties, the magnetic field at the desired launching point and at the plasma current center of gravity, and finally the position of the latter. The different tests that will be carried out will bear on the relative distances of these points.

4.1 Magnetic field stable minima

The magnetic field map that is retained for the entirety of our development is the one corresponding to the time of plasma breakdown, for obvious reasons. The values of interest here are the positions of the minima of the module of the poloidal magnetic field B. There are different ways to calculate them, but the retained one consists in using the derivatives of B^2 along both directions r and z:

$$\frac{dB^2}{dr} = 2 \cdot \left(B_r \frac{dB_r}{dr} + B_z \frac{dB_z}{dr} \right) \tag{29}$$

$$\frac{dB^2}{dz} = 2 \cdot \left(B_r \frac{dB_r}{dz} + B_z \frac{dB_z}{dz} \right) \tag{30}$$

where B_r and B_z are the components of B along each direction. The advantage of formulae (29) and (30) is that each term is easily expressed as the product of a precalculated matrix and the current vector formed by $I_a(t_0)$ and $I_e(t_0)$. In order to remove the saddle points and to directly obtain the minima, the implemented algorithm searches for a simultaneous change of sign of the derivatives from the minus to the plus sign. As experience has shown that the low magnetic field regions are often very close to the smallest available radius, an edge condition of $\left.\frac{dB^2}{dr}\right|_{r=r_{min}} < 0$ has been set. To remove irrelevant minima, only those which correspond to a value of B smaller than the half of the mean of B are kept. As indicated by the title of this section, the purpose here is not only to find the minima of the magnetic field map, but also to sort out those that are stable with respect to plasma confinement. The stability condition (i.e. existence of a callback force with respect to the equilibrium position) is given by:

$$\text{sign}(\frac{dB_z}{dr}(r,z)) = \text{sign}(I_p) \tag{31}$$

The next step is thus to filter out the minima that occur in unstable zones. However, this condition being very strong, we must reduce its strength by adding (or subtracting) the error on the derivative. The latter is simply calculated using (26).

The second parameter that must be calculated for each minimum is an indicator of its extension in the poloidal section. This parameter must not only give information on the size of the weak field zone but simultaneously account for the inaccuracy on its exact position. The mathematical formulation consists in setting this parameter as being the radius r_{zone} of a circle centered on the minimum position. This circle can be imagined as the intersection of a sphere, whose radius R_{Lap} corresponds to the curvature of B at the minimum, with a horizontal plan placed at a vertical distance from the pole of the sphere given by the normalized error on B at the minimum. The formula goes as follows:

$$r_{zone} = R_{Lap}\sqrt{1 - \left(1 - \frac{\Delta B(r_{min}, z_{min})}{\Delta B_{max}}\right)^2} \tag{32}$$

where

$$R_{Lap} = \sqrt{\frac{B_{mean}}{\nabla^2 B(r_{min}, z_{min})}} \tag{33}$$

The formulation (32) combines both requests as r_{zone} increases if R_{Lap} or ΔB increases. Its disadvantage however is that it is very sensitive to the

inaccuracy on B, and thus a very localized minimum can have a big extension if it occurs in a zone of poor reliability. The expression (33) for the radius of curvature is given by a mixture of dimensional analysis, normalization constraint and mathematical measurement of the curvature (introduced by the Laplacian here).

In our treatment, a direct evaluation of the minimum of B in the stable zone is done and can be used as a test for the quality of the previous procedure.

4.2 Other parameters and testing

4.2.1 Plasma current center of gravity

As far as the plasma current is concerned, the most interesting parameter is the position of its center of gravity in function of time, and more precisely just after t_0. Ideally, one would compute the trajectory directly from t_0+1 and use the first calculated position as the reference for the analysis of correlations between the magnetic field structure and the plasma behaviour. However, the inaccuracies in the very beginning of the existence period of the plasma are too big and it is not rare that, despite all the efforts made against it, the behaviour of the plasma is not physical at that time (e.g. the position of the center of gravity calculated as being out of the Tokamak's section). In consequence, the threshold value of 4000 A for I_p is used to fix what can be considered as the beginning time t_{CG} of reliable information on the plasma current center of gravity. The underlying hope while using such an approximation is that the plasma position does not evolve too much between t_0 and t_{CG}, such that the analysis on the magnetic field structure at t_0 is still relevant with respect to the position of the plasma center of gravity at t_{CG}. In this problematics, one must also keep in mind that we have to analyze the magnetic field at the last moment when we are still sure that there is no plasma present (and hence not at t_{CG}). The reasons for that are firstly that the analysis must bear on a magnetic field structure that is perfectly controllable, and thus plasma free, in order to have the possibility to elaborate a strategy anterior to the experiment. Secondly, the possible presence of plasma is a source of noise on the magnetic field values and thus reduces their accuracy, which is already at the limit of the acceptable. Finally, the equilibrium procedure (or the plasma itself by the mean of the current it carries) will automatically generate a magnetic field structure that is stable with respect to plasma confinement, and hence change dramatically the information on the initial magnetic situation.

The radius r_{CG} of the error disk on the position of the center of gravity

has been calculated with a combination of its mean deviation $\bar{\sigma}_{CG}$ and of the resolution achieved by the model. The latter corresponds approximately to a quarter of a pyramidal finite element, which can be calculated in terms of radius as the quarter of the diagonal d of an element. It finally gives:

$$r_{CG} = \sqrt{\bar{\sigma}^2_{rCG} + \bar{\sigma}^2_{zCG}} + \frac{1}{4}d \tag{34}$$

4.2.2 Launching point

The launching point is the point of the section corresponding to the desired initial position for the center of gravity. It is defined before the shot, and the confinement algorithm firstly drives the plasma towards it as if it were a stable equilibrium position for a 2-D motion. The uncertainty on its exact position is set as the maximum resolution of our model, that is the mean distance between two x-grid points.

4.2.3 Testing

A whole set of tests is built on the different parameters described above. The questions that are answered by these tests are questions of correlations between the weak $B-$field zones, the initial center of gravity position and the launching point position. As for B, a zone of possible presence is built for the center of gravity and the launching point, using their respective uncertainty. The program then tests the overlaps of the zones by comparing the distances between the different points with the sizes of the zones. For each minimum of the magnetic field, a value corresponding to the kind of overlap is attributed to a parameter that will serve later on as random variable. This parameter hence summarizes the global behaviour of the experiment. One of the problem encountered here is the plurality of the minima of B. There are two options in order to manage with it. The first one consists in including all of them in the statistical analysis, leading us so to a complete but complex treatment and hiding the relevance problem of certain minima in the great number of shot used for the analysis. The second possibility requires an initial choice on the minima and the attribution of a unique solution per shot. This implies the delicate construction of a quality factor for the minima but eliminates the problems of relevance and complexity. The impact of the choice of the quality factor could also be studied *a posteriori* on the results obtained by the analysis in different cases. The arguments that should be used for such a factor are the deepness and the extension of the minimum. A good minimum for plasma creation would then be required to be deep and

extended. Formally, the quality factor q could be expressed as:

$$q = R_{Lap} \cdot \frac{B_{mean}}{B(r_{min}, z_{min})} \tag{35}$$

Note that the normalization by B_{mean} is used in (35) to have the possibility to compare these factors between shots. R_{Lap} has been used instead of r_{zone} to prevent the quality factor from being distorted by the error on the position.

4.3 Results and discussion

An example of the most advanced result obtained so far is given in figure 11. This figure represents the constant magnetic field contours at t_0, with their corresponding amplitudes (given by the color bar, in Tesla). The red crosses correspond to the stable minima found by derivation, while the red star gives the position of the smallest $B-$field in the stable zone. The trajectory of the plasma current center of gravity is shown for the times from t_p (i.e. $I_p \geq 4000\,\mathrm{A}$) to the time when the plasma current is maximum. It is represented by the black solid line starting with a blue circle. The other two blue circles delimit the corners of a virtual square that would contain the error disk on the initial position. The green cross corresponds to the initial desired position for the center of gravity. The quantitative parameters for the magnetic field minima and the center of gravity are given in table 2.

Kind	**r [m]**	**z [m]**	**B [T]**	**$\mathbf{r}_{zone}$ [m]**	**q**
B_w	0.6140	0.1425	0.0006	0.1684	3.47
B_{m1}	0.6550	0.1425	0.0007	0.1939	3.98
B_{m2}	0.6140	-0.1425	0.0018	0.5640	3.77
CG	0.8579	0.0410	0.0023	0.08	–

Table 2: Results of the developed algorithm for the direct minimum of B, B_w, two minima found by the derivative method, B_{m1} and B_{m2}, and the center of gravity CG. The studied case here is the shot 25 016, with an eigenmode representation. It corresponds to figure 11.

The testing results for B_{m1} and B_{m2}, both minima obtained by the derivative method, are the following. For B_{m1}, the launching point belongs to the zone corresponding to the minimum, but the zone of the center of gravity does not overlap any of them. By looking at figure 11, one can see that the zones corresponding to the center of gravity and to B_{m1} are however not so

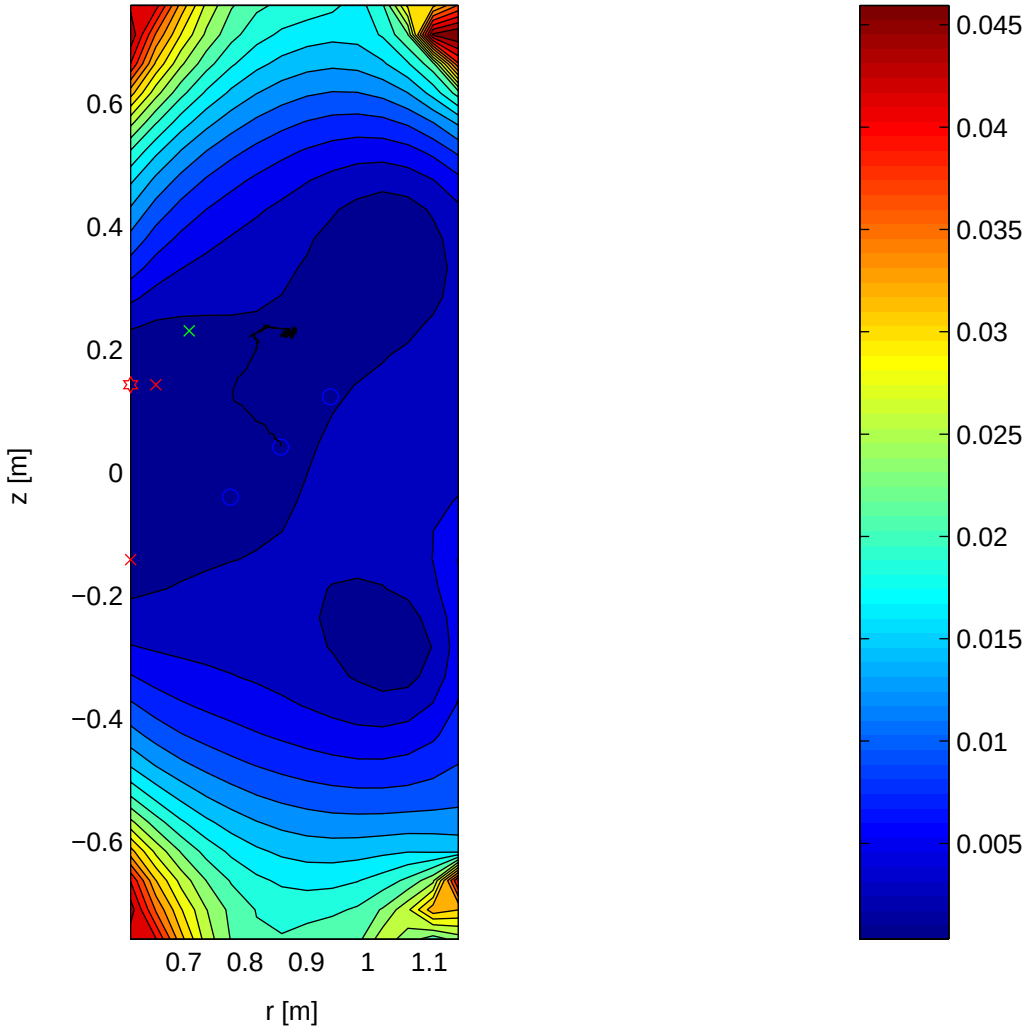

Figure 11: Constant magnetic field contours at t_0 (in Tesla), stable minima found by derivation (red crosses), smallest $B-$field in the stable zone (red star), trajectory of the plasma current center of gravity (black solid line) from t_p (i.e. $I_p \geq 4000\,\mathrm{A}$) to the time when the plasma current is maximum. The blue circles delimit the corners of a virtual square that would contain the error disk on the initial position. The green cross corresponds to the initial desired position for the center of gravity.

far from each other. The proximity between B_{m1} and B_w also proves that the derivative method is efficient. The obtained values for the quality factor q given in table 2 indicates an optimum for B_{m1}. A glance at figure 11 confirms that B_{m1} is effectively the best candidate for our study, which is reassuring for the using of such a quality factor in the selection of minima. As far as B_{m2} is concerned, it is firstly observed that the corresponding amplitude of B is approximately three times the minimum calculated amplitude. Secondly, the associated radius covers nearly half a cross section, which is clearly too big. The existence of minima as B_{m2} hence clearly establishes the requirement of a process of selection of minima during the statistical analysis.

All that has been said about the shot used here has also been checked for other cases. The removal of the unphysical I_b's has been verified *a posteriori*, and the process effectively leads to a solution where the remaining I_b's are well juxtaposed.

5 Conclusions

The work that has been carried out to obtain the actual modelisation has allowed to identify and solve many problems of stability with respect to the choice of parameter, and to enhance considerably its generic character. In the present state, the differences between the cases with or without eigenmodes are negligible in the magnetic map or in the center of gravity trajectory. In addition, the choice of weights is now fairly optimized and also have good generic features. As far as plasma current modelisation is concerned, the applied method can be considered to be efficient in the removal of unphysical solutions, and also increases strongly the resolution on the center of gravity position. Further developments will consist in reducing the time interval considered in the solving, and also in increasing the number of finite elements per columns so that they become nearly squared. By this way, the fact of considering a circular shape for the error on the position of the center of gravity would have more sense. Another improvement would also be to add a juxtaposition test on the process of choice of the finite elements.

As far as error calculation is concerned, the work done shows that even if the uncertainties on the observables are of the same order of size as the observables themselves in the interesting time interval, they are rarely bigger. Besides, the stability of the model with respect to the choice of parameters shows that despite the inaccuracies, the found solutions can be trust to a certain extent. Both arguments seem to be a very good omen for the results that will come out of the statistical analysis. The latter will effectively reduce the inaccuracies by the big number of shots that will be involved. Appended to this report, you can find the latest version of the program used to generate the results given throughout the text.

References

[1] J.-M. Moret *et al.*, Magnetic measurements on the TCV Tokamak, Rev. Sci. Instrum., Vol. **69**, 6, p. 2333, 1998

[2] J.-M. Moret *et al.*, Breakdown in a continuous low resistivity vessel in TCV, 23rd EPS Conf. on Cont. Fusion and Plasma Phys., Kiev, 1996